Stem Cell Reports
Article

ISSCR

OPEN ACCESS

Endogenous neural stem cells modulate microglia and protect against demyelination

Béatrice Brousse,[1] Océane Mercier,[1] Karine Magalon,[1] Fabrice Daian,[1] Pascale Durbec,[1] and Myriam Cayre[1,*]
[1]Aix Marseille Univ, CNRS, Developmental Biology Institute of Marseille (IBDM), IBDM-UMR 7288, Case 907, Parc Scientifique de Luminy, Marseille Cedex 09 13288, France
*Correspondence: myriam.cayre@univ-amu.fr
https://doi.org/10.1016/j.stemcr.2021.05.002

SUMMARY

In response to corpus callosum (CC) demyelination, subventricular zone-derived neural progenitors (SVZdNPs) are mobilized and generate new myelinating oligodendrocytes (OLG). Here, we examine the putative immunomodulatory properties of endogenous SVZdNPs during demyelination in the cuprizone model. SVZdNP density was higher in the lateral and rostral CC regions, and demyelination was inversely correlated with activated microglial density and pro-inflammatory cytokine levels. Single-cell RNA sequencing showed that CC areas with high levels of SVZdNP mobilization were enriched in a microglial cell subpopulation with an immunomodulatory signature. We propose MFGE8 (milk fat globule-epidermal growth factor-8) and β3 integrin as a ligand/receptor pair involved in dialogue between SVZdNPs and microglia. Immature SVZdNPs mobilized to the demyelinated CC were found highly enriched in MFGE8, which promoted the phagocytosis of myelin debris *in vitro*. Overall, these results demonstrate that, in addition to their cell replacement capacity, endogenous progenitors have immunomodulatory properties, highlighting a new role for endogenous SVZdNPs in myelin regeneration.

INTRODUCTION

Myelin regeneration has been observed in the brains of patients with multiple sclerosis, but it is highly variable and not always effective (Albert et al., 2007; Patrikios et al., 2006). In rodents, spontaneous remyelination after experimentally induced demyelination is highly efficient and can involve both parenchymal oligodendrocyte progenitor cells (pOPC) (Franklin et al., 1997; Gensert and Goldman 1997; Zawadzka et al., 2010) and adult neural stem/progenitor cells derived from the subventricular zone (SVZdNPs) (Aguirre et al., 2007; Menn et al., 2006; Nait-Oumesmar et al., 1999; Picard-Riera et al., 2002). In physiological conditions, neural stem cells (NSC) in the adult SVZ divide slowly and asymmetrically to give rise to actively proliferating progenitors (C cells), which give rise mostly to neuroblasts, but also, at a much lower frequency, to oligodendrocyte progenitor cells (OPC) (Doetsch et al., 1999; Menn et al., 2006). The induction of demyelination in the periventricular white matter leads to a quadrupling of OPC production in the SVZ (Menn et al., 2006). SVZdNPs have long been considered to make a much smaller contribution to spontaneous remyelination than pOPC, but two independent studies revealed an unexpectedly high and regionalized mobilization of these cells during cuprizone-induced demyelination in mice (Brousse et al., 2015; Xing et al., 2014).

Several studies of NSC grafts in injured rodent brain have reported a bystander effect of NSC independent of cell replacement, via the production of neurotrophic factors (Goldberg et al., 2015; Zuo et al., 2015), and immunomodulation. NSC can dialogue with infiltrating T cells from the bloodstream and microglial cells (Cusimano et al., 2012; Martino et al., 2011; Pluchino et al. 2005, 2009; Zhang et al., 2016).

Microglia play key roles in demyelination/remyelination events (Chu et al., 2018). Activated microglia can cause cell damage by producing cytokines and nitric oxide. However, they are also involved in phagocytosis and the removal of myelin debris, a prerequisite for successful remyelination (Kotter et al., 2006; Lampron et al., 2015; Poliani et al., 2015). Microglial cells are activated following demyelination, and can adopt different phenotypes, from M1 (pro-inflammatory) to M2 (immunomodulatory), with many possible intermediate states (Lloyd et al., 2019; Miron et al., 2013; Peferoen et al., 2015; Vogel et al., 2013). Several studies have suggested that NSCs can promote the polarization of microglial cells toward the M2 phenotype. However, these properties were demonstrated either after the transplantation of hundreds of thousands (or even millions) of NSCs (Gao et al., 2016; Marteyn et al., 2016), or in co-culture experiments performed *in vitro* (Liu et al., 2013; Wu et al., 2014).

In this study, we investigated whether and how endogenous SVZdNPs spontaneously recruited to demyelinated lesions can also act through immunomodulation. An analysis of corpus callosum (CC) areas with high or low levels of SVZdNP recruitment revealed that the presence of SVZdNPs was associated with the degree of demyelination and an inflammatory signature. Single-cell RNA sequencing on microglial cells sorted from these different CC areas revealed clusters of cells enriched in M1 or M2

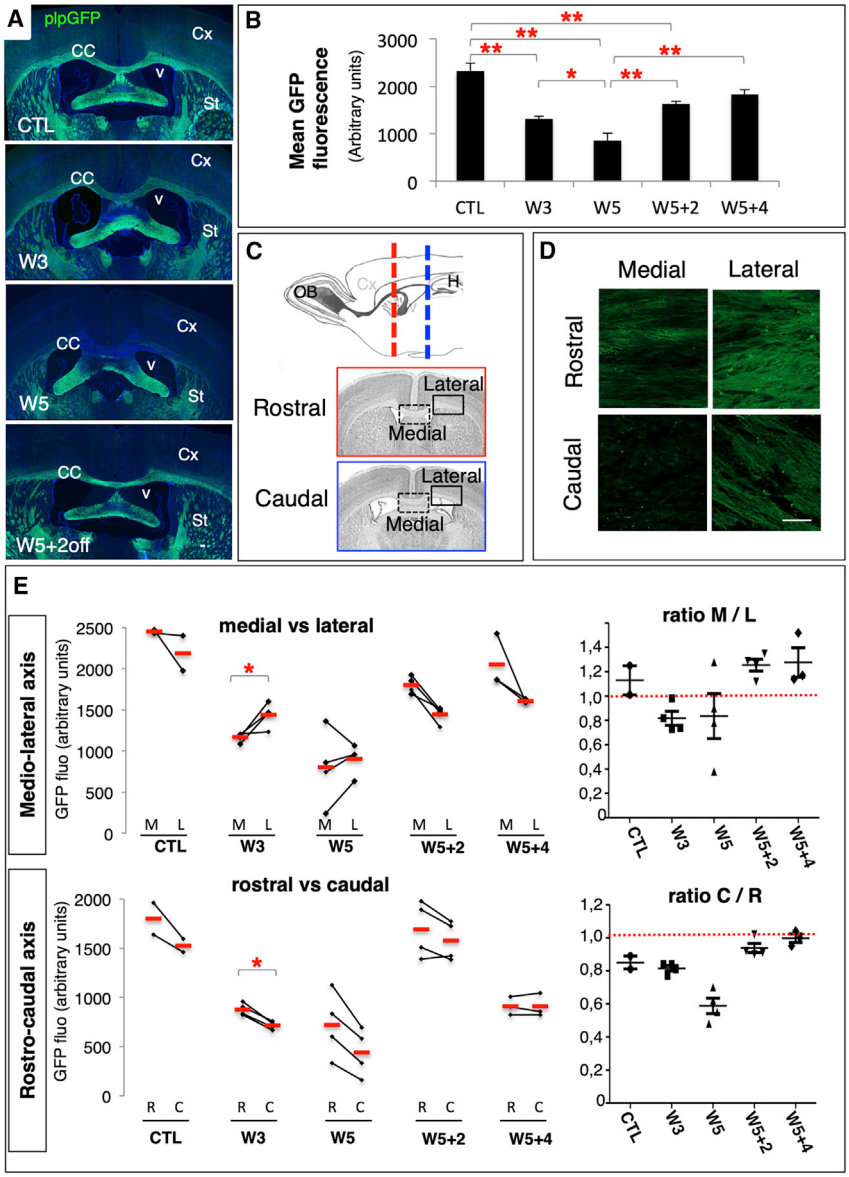

Figure 1. Differential demyelination within the corpus callosum following cuprizone treatment

(A and B) Illustration (A) and quantification (B) of demyelination and remyelination in plpGFP mice fed cuprizone (GFP fluo mean ± SEM; n = 4 mice per time point).

(C) Representation of the areas analyzed in the corpus callosum. Rostral (Bregma +0.5 to +1) and caudal (Bregma −0.3 to −0.8) levels are illustrated, together with the medial CC (between the ventricles) and lateral CC (above the ventricles).

(D) Myelin labeling (plpGFP mice) in the various CC areas after 5 weeks of cuprizone treatment.

(E) Quantification of the GFP signal in plpGFP mice, in the medial (M) relative to lateral (L) CC (upper panel) and in the caudal (C) relative to rostral (R) CC (lower panel), during cuprizone-induced demyelination and remyelination. A ratio of 1 means that myelin contents are similar in the medial and lateral CC (upper right panel) or in the rostral and caudal CC (lower right panel). Red dashes indicate the means; n = 3 to 4 mice per time point. Ratios are expressed as mean ± SEM. For multiple group comparisons (A) ANOVA by score permutation was performed, followed by Kruskal-Wallis tests; for comparisons between two brain areas (paired samples, as in E), Wilcoxon tests were performed. *p < 0.05; **p < 0.01. Scale bar: 100 μm.

genes, suggesting the existence of an immunomodulatory phenotype in a population of microglial cells located in areas in which SVZdNPs were abundant. Finally, we identified MFGE8 as a candidate factor secreted by SVZdNPs for improving the phagocytotic properties of microglia.

RESULTS

Cuprizone-induced demyelination and SVZdNP mobilization are regionalized within the corpus callosum

Cuprizone is known to trigger diffuse demyelination throughout the brain. As expected, 3 weeks after the initiation of cuprizone treatment, CC myelin content (assessed by GFP signal in PLP-GFP mice) decreased, reaching a minimum after 5 weeks of treatment, and then gradually recovering to normal levels after return to a normal diet (Figures 1A and 1B). We assessed the degree of demyelination along the rostrocaudal and mediolateral axes of the CC (Figures 1C and 1D). Control mice not exposed to cuprizone had a slightly higher myelin content medially (GFP ratio medial/lateral = 1.13 ± 0.12) and rostrally (GFP ratio caudal/rostral = 0.85 ± 0.04) (Figure 1E). During cuprizone exposure, myelin loss was more pronounced in the medial and caudal CC (Figures 1D and 1E). Indeed, at W3, the GFP signal was weaker in the medial CC than in the lateral CC in all mice, and the medial/lateral fluorescence ratio

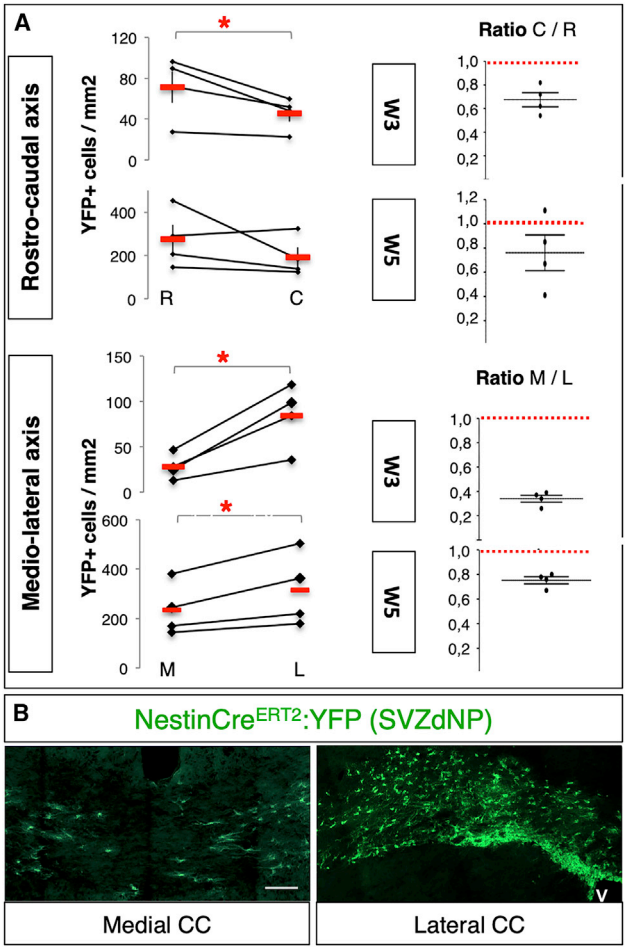

Figure 2. SVZdNP mobilization is regionalized within the CC following cuprizone treatment

(A) Quantification of SVZdNP mobilization along the rostrocaudal and mediolateral axes after 3 (W3) and 5 weeks (W5) of exposure to cuprizone. The density of YFP$^+$ cells within each mouse is compared between the rostral (R) and caudal (C) CC (upper panels) and between the lateral (L) and medial (M) CC (lower panels). Red dashes indicate the means, n = 4 mice per time point. Ratios are expressed as mean ± SEM.

(B) Illustration of SVZdNP mobilization after 5 weeks of cuprizone treatment in NestinCre^{ERT2}:YFP mice. The medial (left panel) and lateral CC (right panel) are shown. Scale bar: 100 μm. For comparisons between two brain areas (paired samples), Wilcoxon's tests were used. *p < 0.05. See also Figure S1.

decreased to 0.82 ± 0.06 (p = 0.02). After 5 weeks of dietary supplementation with cuprizone (W5), demyelination became heterogeneous along the rostrocaudal axis, with the caudal areas more strongly affected and a decrease in caudal/rostral fluorescence ratio to 0.58 ± 0.05 (p = 0.03). Thus, during cuprizone-induced demyelination, the rostral and lateral CC lose less myelin than the caudal and medial CC. After the cessation of cuprizone supplementation and remyelination, these regional differences in myelin content disappeared, with myelin levels returning to control levels everywhere (Figure 1E).

Having previously shown that SVZdNPs preferentially contribute to rostral CC remyelination (Brousse et al., 2015), we traced SVZdNPs in NestinCre^{ERT2}:rosaYFP transgenic mice, examining their distribution along both the rostrocaudal and mediolateral axes and calculating density ratios for each animal during demyelination. In control mice, SVZdNPs were almost entirely absent from the CC (Brousse et al., 2015). As early as W3, SVZdNPs were preferentially recruited to the rostral and lateral CC (Figure 2A, p = 0.03). This differential recruitment was more pronounced along the mediolateral axis, with far fewer SVZdNPs present in the medial CC than in the lateral CC (28.5 ± 7.0 vs. 84.6 ± 17.6 YFP + cells/mm^2; medial/lateral ratio = 0.31 ± 0.04; p = 0.03) (Figure 2A). This regionalized distribution of SVZdNP was maintained, albeit to a lesser extent, at W5 (234.5 ± 53.1 vs. 316.0 ± 73.9 YFP + cells/mm^2; medial/lateral ratio = 0.75 ± 0.03; p = 0.03) (Figures 2A and 2B).

The recruitment of SVZdNPs to the demyelinated CC thus followed a regionalized pattern, with these cells preferentially recruited to the rostrolateral CC, just above the SVZ niche. These areas correspond to those least affected by cuprizone-induced demyelination (Figures 1D and 1E), suggesting that they may be either protected from demyelination or that remyelination may begin more rapidly in these areas, even in the presence of cuprizone. At W3, 9.8% ± 1.2% of SVZdNPs already differentiated into mature (CC1+) OLG (oligodendrocyte), and up to 30.2% ± 3.0% at W5 (Figure 3A). Yet, the use of NestinCre^{ERT2}:mTmG mice (membrane GFP allowing OLG shape and myelin segment visualization) showed that these young OLGs do not yet display the typical morphology of myelinating OLG (Figures S1A′–S1B″). By contrast, after cuprizone removal SVZ-derived OLG exhibit MBP + myelin segments (Figures S1C′–S1C″).

Thus, during cuprizone-induced demyelination, SVZdNPs are recruited to the CC, where they rapidly adopt an OLG identity. However, the efficient remyelination of axons by these cells does not begin until cuprizone exposure ceases. Early SVZdNP maturation into myelinating OLG is not, therefore, sufficient to account for the differential myelin content of different parts of the CC at W3. We therefore hypothesized that the rostral and lateral CCs were protected against demyelination.

A significant proportion of SVZdNPs remain undifferentiated in the demyelinated CC

SVZdNPs rapidly adopted an OLG fate following their recruitment to the demyelinated CC, but a significant proportion of YFP$^+$ SVZdNPs nevertheless remained negative

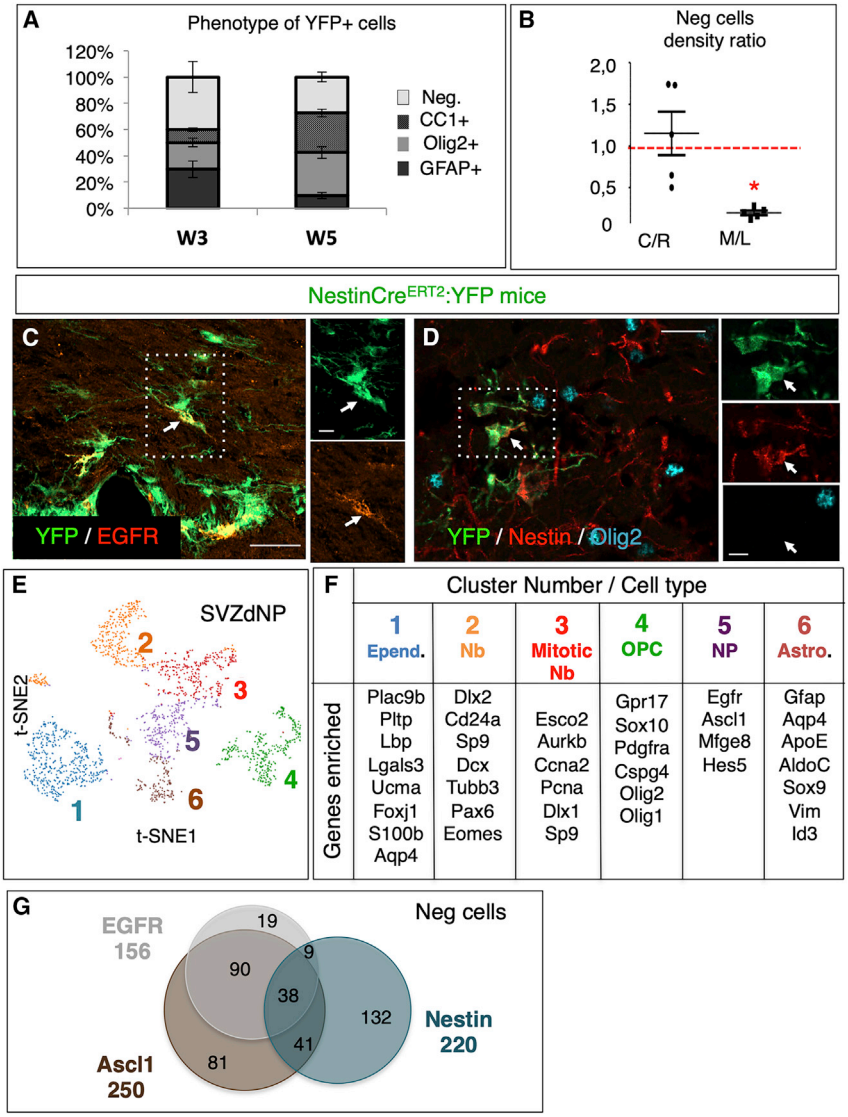

Figure 3. A significant proportion of SVZdNPs remain undifferentiated in the demyelinating corpus callosum

(A) Phenotype of the SVZdNPs mobilized in the CC during cuprizone-induced demyelination; n = 4 mice at each time point. Graph shows means ± SEM.

(B) Relative densities of immature cells (lineage-neg cells) in the medial and lateral CC (M/L ratio) and in the caudal and rostral CC (C/R ratio). Immature cells mobilized from the SVZ are more numerous in to the lateral than medial CC, as indicated by the mean ratio <1; n = 4 mice. Ratios are expressed as mean ± SEM.

(C and D) EGFR (C) and Nestin (D) immunolabeling in NestinCre^{ERT2}:YFP mice exposed to cuprizone. Arrows indicate YFP$^+$ EGFR$^+$ cells (C) and YFP$^+$ Nestin$^+$ Olig2$^-$ cells (D). The cells in the white squares are shown at higher magnification.

(E) t-SNE and automated clustering after single-cell RNA sequencing of SVZdNP sorted from the CC of NestinCre^{ERT2}:YFP mice fed cuprizone for 4 weeks (n = 5 mice; 1931 sorted cells).

(F) Identification of the six clusters generated by automated clustering, with a list of enriched genes for each cluster.

(G) Venn diagram illustrating the expression of type C cell markers among lineage-negative cells. The numbers are the total numbers of lineage-negative cells expressing *Egfr, Nestin, Ascl1,* or any combination of these three progenitor markers.

Scale bars: 20 μm, magnification: 5 μm. For comparisons between two brain areas (paired samples), Wilcoxon tests were performed. *p < 0.05.

for OLG (CC1, Olig2), astrocytic (GFAP) or neuronal (DCX) markers (40.1% ± 9.9% and 27.4% ± 3.7% at W3 and W5, respectively, referred to hereafter as "lineage-neg cells") (Figure 3A). During demyelination, the density of lineage-neg cells was significantly higher in the lateral than in the medial CC, with a ratio medial/lateral ratio of 0.2 ± 0.03 (p = 0.02) (Figure 3B). Some of these cells expressed EGFR or Nestin, markers of C cells and neural progenitor cells, respectively (Figures 3C and 3D). We characterized the SVZdNPs mobilized in the demyelinated CC in more detail, by single-cell RNA sequencing. The CC of NestinCre^{ERT2}:YFP mice fed cuprizone for 4 weeks was dissected and YFP$^+$ cells (SVZdNP) were sorted by FACS. Following t-distributed stochastic neighbor-embedding (t-SNE) projection and automated clustering, the 1931 SVZdNP were ordered into six distinct clusters (Figure 3E). Enrichment in the expression of typical markers made it possible to identify each cluster (Figure 3F): (1) ependymal cells, (2) neuroblasts, (3) proliferative neuroblasts, (4) OPC, (5) neural progenitors, and (6) astrocytes. We focused on lineage-neg cells by excluding all cells expressing typical markers of ependymal cells and of the three neural lineages, on the basis of Plac9b (ependymal cells), Ldh1l1, S100B (astrocytes), DCX, Sp9 (neuroblasts), and Sox10 (OPC/OLG) expression. We then determined the proportion of the remaining 750 cells (corresponding to 39% of the total cell population) expressing typical markers of SVZ neural progenitors ("type C" cells): EGFR, Nestin, and/or Ascl1. The lineage-neg SVZdNP recruited to the demyelinated CC were found to have the phenotypic characteristics of immature neural progenitor cells: 55% (410/750) of the lineage-neg cells expressed at least one of the three markers

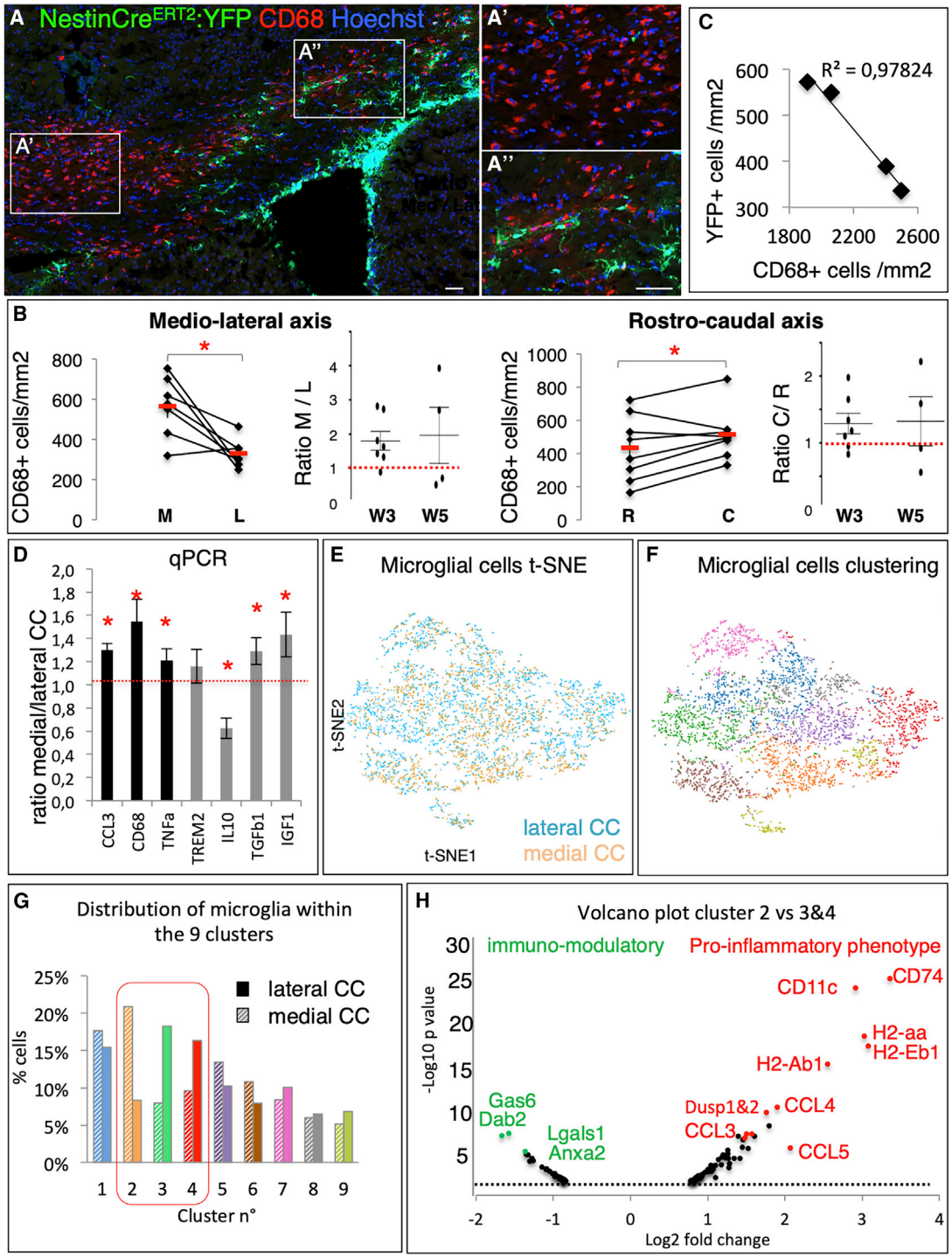

Figure 4. The inflammatory signature varies along the lateromedial axis in the demyelinated corpus callosum

(A) Illustration of activated (CD68$^+$) microglia in the CC of mice fed *with* cuprizone for 3 weeks. The white boxes in the medial (A′) and lateral CC (A″) are shown at higher magnification.

(B) Quantification of CD68$^+$ microglia density in the medial (M) relative to lateral (L) CC (left panels) and in the caudal (C) relative to rostral (R) CC (right panels). Red dashes indicate the means, n = 7 mice at W3 and 5 mice at W5. Ratios are expressed as mean ± SEM.

(C) Inverse correlation between activated microglia and SVZdNP density in the CC of NestinCre^{ERT2}:YFP mice fed cuprizone for 3 weeks (n = 4 mice).

(legend continued on next page)

(EGFR, Ascl1, or Nestin), and 9% of these cells (38/410) expressed all three simultaneously (Figure 3G). Thus, after cuprizone treatment, the CC contained a significant proportion of SVZdNPs that retained the characteristics of immature progenitors.

The density of activated microglial cells in the demyelinated CC is inversely proportional to SVZdNP mobilization

NSCs grafted into injured brain have been shown to have immunomodulatory properties (Kokaia et al., 2012). We therefore hypothesized that the SVZdNPs that remained immature in the demyelinated CC might provide protection against demyelination by modulating the inflammatory microenvironment. We first investigated the distribution of microglial cells. In control conditions, microglial cells were homogeneously distributed along the CC (Figures S2A and S2B) and CD68 expression was almost undetectable (Figure S2C). After 3 weeks of cuprizone exposure, the numbers of total (CX3CR1+; Figures S2C and S2D) and activated (CD68+) microglial cells were significantly higher in the medial than in the lateral CC (563.6 ± 56.9 vs. 329.0 ± 26.7 $CD68^+$ cells/mm^2; medial/lateral ratio = 1.81 ± 0.27, p = 0.012; Figures 4A and 4B). The increase in microglial density in the medial CC was associated with a 2.3-fold increase in the level of proliferating CD68 cells relative to the lateral CC (Figures S2D–S2G; p = 0.03). Similarly, activated microglial cells were more numerous in the caudal than the rostral CC (514.9 ± 54.3 vs. 433.4 ± 70.2 $CD68^+$ cells/mm^2; caudal/rostral ratio = 1.32 ± 0.14, p = 0.025) (Figure 4B). This regionalization was no longer significant at W5 (caudal/rostral ratio: 1.37 ± 0.37 p = 0.23; medial/lateral ratio: 1.97 ± 0.82 p = 0.36; Figure 4B). Interestingly, areas enriched in SVZdNPs had smaller numbers of activated microglial cells. Moreover, the animals with the highest levels of SVZdNP mobilization in the CC had the lowest density of activated microglia, highlighting a strong inverse correlation (R^2 = 0.978) (Figure 4C). Thus, the areas of the CC resistant to demyelination during cuprizone are rich in SVZdNPs and contain few activated microglia.

The inflammatory signature varies along the lateromedial axis in the demyelinated CC

We investigated the ability of SVZdNPs to modulate microglial cell activation, thereby exerting protective functions, by first determining whether the different areas of the CC were associated with a particular inflammatory signature.

We performed qPCR analyses on animals fed cuprizone for 3 weeks. The findings confirmed CD68 enrichment and showed that the level of expression of two pro-inflammatory cytokines, CCL3 and tumor necrosis factor-α, was significantly higher in the medial than the lateral CC (p = 0.04 and 0.02, respectively; Figure 4D).

We found that the level of expression of the anti-inflammatory cytokine IL10 was significantly lower in the medial CC (medial vs. lateral ratio: 0.63 ± 0.09, p = 0.02; Figure 4D). By contrast, the medial CC was found to be enriched in insulin growth factor 1 and transforming growth factor-β1, two well-known immunomodulatory factors. Thus, during demyelination, CC areas with low levels of SVZdNP mobilization seem to have a more inflammatory profile than areas with high levels of SVZdNP recruitment.

For comparison of the molecular signatures of microglia in the medial and lateral CC during demyelination, microglia from CX3CR1GFP mice fed cuprizone for 4 weeks were sorted by FACS and subjected to single-cell RNA sequencing. The medial and lateral microglial samples did not segregate clearly on the t-SNE projection (Figure 4E). However, the clustering ordered the microglial into nine clusters (Figure 4F) with a differential distribution of microglia from the medial and lateral CC for clusters 2, 3, and 4, but not for the other clusters (Figure 4G). We characterized these specific clusters (corresponding to 40.8% of all microglial cells analyzed) further, by comparing the cluster enriched in medial microglia (Cluster 2) with the two clusters enriched in lateral microglia (Clusters 3 and 4) and identifying the genes displaying differential expression, with a 2-fold change cutoff. In total, 13 genes were downregulated and 40 genes were upregulated in cluster 2 relative to clusters 3 and 4.

Almost all the enriched genes in cluster 2 (in which microglial cells from the medial CC predominate) encode

(D) RT-qPCR analysis of cytokine expression in the medial and lateral CC. Black and gray columns represent inflammatory and immunomodulatory cytokines, respectively (n = 5 mice). Graph shows mean ± SEM.

(E) t-SNE representation after single-cell RNA sequencing of microglial cells sorted from the medial (2,133 cells, in orange) and lateral CC (2,304 cells, in blue) after 4 weeks of cuprizone treatment (n = 4 mice).

(F) Unbiased automated clustering segregating microglial cells into nine clusters, represented by different colors.

(G) Distribution of microglia from the medial and lateral CC in each of these nine clusters. Cluster 2 is enriched in cells from the medial CC, whereas clusters 3 and 4 are enriched in cells from the lateral CC.

(H) Comparison of gene expression profiles between cluster 2 and clusters 3 and 4, represented as a volcano plot. In red, genes significantly upregulated in cluster 2 corresponding to M1 markers; in green, genes significantly upregulated in clusters 3 and 4 corresponding to M2 markers. Scale bars: 50 μm. For comparisons between two brain areas (paired samples, as in B and D), Wilcoxon tests were performed. *p < 0.05. See also Figures S2 and S3.

pro-inflammatory cytokines (CCL3, CCL4, CCL5) or proteins involved in antigen presentation (H2-aa, H2Ab1, H2-Eb1, CD74) characteristic of the M1 phenotype (Figure 4H). Conversely, the enriched genes in clusters 3 and 4 (in which microglial cells from the lateral CC predominate) are immunomodulatory genes characterizing the M2 phenotype (Gas6, Dab2, Lgals1, Anxa2) (Figure 4H). Pathway analysis with EnrichR confirmed that the genes displaying enrichment in cluster 2 were indeed linked to the inflammatory response, and cytokine/chemokine activity (Figure S3).

Thus, a large population of microglia in the medial CC adopts a pro-inflammatory phenotype with deleterious effects on myelin integrity and repair, whereas a subpopulation of microglia in the lateral CC displays an immunomodulatory phenotype associated with neuroprotection and regeneration.

Identification of ligand-receptor pairs involved in the dialogue between SVZdNP and microglia

We used our single-cell RNA sequencing data, focusing on secreted extracellular molecules or membrane receptors reported to have immunomodulatory properties in the Gene Ontology database, to identify candidate ligand-receptor pairs for involvement in SVZdNP/microglia dialogue.

According to the literature (De Feo et al., 2012; De Gioia et al., 2020), immature neural progenitors (cluster 5 in Figures 3E and 3F) are the SVZdNP population most likely to display immunomodulatory properties. The three genes displaying the most significant enrichment in cluster 5 (Figure 3F) were *Egfr* (2.7-fold; $p = 1.41 \times 10^{-16}$), *Mfge8* (2.7-fold; $p = 5.87 \times 10^{-13}$), and *Ascl1* (2.1-fold; $p = 2.80 \times 10^{-1}$). MFGE8 (milk fat globule-epidermal growth factor-8) and its receptor, β3 integrin (ITGB3), are known to induce the phagocytosis of apoptotic cells and to act as "endogenous protective factors" for various brain lesions (Deroide et al., 2013; Liu et al., 2015; Xiao et al., 2018). *Mfge8* expression was very strong in immature neural progenitors (Figure 5A), and *Itgb3* was expressed in most of the microglial cells present in the demyelinated CC, regardless of localization (medial vs. lateral CC) or t-SNE cluster (Figure 5B).

MFGE8 was detected by immunolabeling in cuprizone-treated mice. MFGE8 is a secreted protein, so the resulting staining was rather diffuse and punctiform, making it difficult to count MFGE8-expressing cells reliably. Nevertheless, MFGE8 was detected in GFP^+ SVZdNP and in microglial cells (Figure 5C). Single-cell analysis on microglial cells showed *Mfge8* levels to be low, with no significant difference between the medial and lateral CC (log_2 fold-change = 0.1274; p-adj = 0.978). Mean fluorescence intensity analyses on the medial and lateral CC showed stronger MFGE8 expression in the lateral than the medial CC (Figure 5D).

Given the mode of action of MFGE8/Itgb3, we hypothesized that the MFGE8 secreted by SVZdNP might promote the endocytosis of myelin debris by microglial cells, which is crucial for the resolution of inflammation. Indeed, the proportion of BV2 microglial cells engulfing CFSE-labeled myelin debris *in vitro* increased by 39% ($p = 0.03$) after the addition of MFGE8 to the culture medium (Figure 5E).

We then cultured SVZ cells as neurospheres from wild-type (WT) and $MFGE8^{-/-}$ mice and collected the conditioned medium, to demonstrate that SVZ progenitors secrete MFGE8 and promote the phagocytosis of myelin debris by microglial cells. SVZ cells from WT mice cultured as neurospheres secreted MFGE8 (Figure S4), and their conditioned medium significantly enhanced the phagocytosis of myelin debris ($p = 0.01$; Figures 5E and 5F). By contrast, conditioned medium from neurospheres derived from mutant mice lacked MFGE8 (Figure S4) and did not promote the phagocytosis of myelin debris (Figure 5F). The addition of MFGE8 to conditioned medium from neurospheres derived from $MFGE8^{-/-}$ mice rescued phagocytosis (Figure 5F).

Together, these results point on remarkable correlations among SVZdNP mobilization, demyelination levels, and microglia phenotype, supporting the hypothesis that SVZdNP mobilized by cuprizone treatment protect against CC demyelination by reducing inflammation and promoting the phagocytosis of myelin debris.

DISCUSSION

The migration of SVZdNPs toward the lesion on demyelination is now well documented. Several studies have reported a contribution of these cells to myelin repair (Brousse et al., 2015; El Waly et al., 2018; Jablonska et al., 2010; Menn et al., 2006; Xing et al., 2014), but others have suggested that they do not produce myelin (Kazanis et al., 2017; Serwanski et al., 2018). It has also been suggested that SVZdNPs are dispensable for myelin repair but protect neurons against degeneration (Butti et al., 2019). We show here than in addition to replacing OLG, SVZdNPs help to limit demyelination by modulating microglial activity and promoting the phagocytosis of myelin debris.

Consistent with the findings of previous studies (Chrzanowski et al., 2019; Steelman et al., 2012; Zhang et al., 2019), we observed regionalized sensitivity to cuprizone-induced demyelination, with lower levels of myelin loss in the rostral and lateral CC. This may indicate protection against demyelination or early remyelination. Our experiments do not support the "remyelination hypothesis": indeed, myelin segments produced by SVZdNP (visualized with the mTmG reporter) are rare at early time points in the CC. Furthermore, the higher myelin content of rostral and

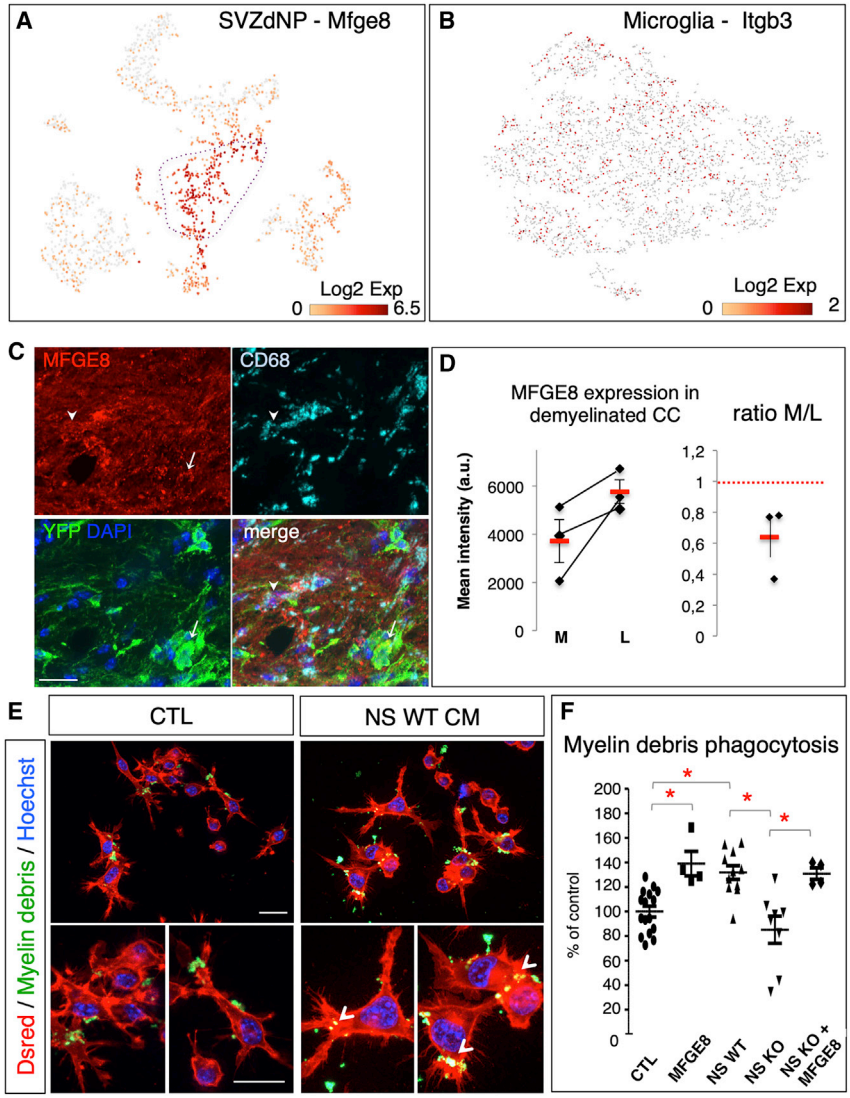

Figure 5. Identification of MFGE8 as a candidate modulator of microglial cells

(A) *Mfge8* expression in SVZdNP, showing an enrichment in neural progenitors (cluster 5, surrounded by a purple dotted line) (n = 5 mice pooled).

(B) Expression of *Itgb3*, encoding the MFGE8 receptor, in microglial cells during cuprizone-induced demyelination (n = 4 mice pooled).

(C) Illustration of MFGE8 expression in the CC of cuprizone-fed mice. Both SVZdNP (arrow) and microglial cells (arrowheads) express MFGE8. Scale bar: 20 μm.

(D) Quantification of the MFGE8 signal (mean fluorescence intensity) in the medial and lateral CC of cuprizone-fed mice (n+ 3 mice). Mean (in red) ± SEM are shown.

(E) Illustration of BV2 microglial cells stably expressing dsRed, cultured in the presence of CFSE-labeled myelin debris, with and without neurosphere (NS)-conditioned medium (CM). Myelin debris taken up by phagocytosis appears as yellow dots in microglial cells (arrowheads). Scale bars: 20 μm.

(F) Quantification of the phagocytosis of myelin debris by microglial cells *in vitro* in control conditions and after the addition of rmMFGE8 or of neurosphere-conditioned medium from WT or MFGE8$^{-/-}$ mice (KO) with or without the addition of rmMFGE8; n = 3 independent cultures, four dishes analyzed per culture. For multiple group comparisons (D) ANOVA by score permutation was performed, followed by Kruskal-Wallis tests. *p < 0.05. See also Figure S4.

lateral areas cannot be attributed to pOPC, which preferentially contribute to remyelination in the caudal and medial CC (Brousse et al., 2015; Xing et al., 2014).

Many studies have shown that NSCs bear cytokine receptors and display homing to inflamed sites (Boockvar et al., 2005; Carbajal et al., 2010). SVZdNPs are, therefore, probably attracted to the demyelinating CC by secreted cytokines. Grafted NSCs contribute to regeneration via bystander effects independent of cell replacement (for review, see Kokaia et al., 2012). They create niches of neural progenitors that trigger the apoptosis of infiltrating T cells (Pluchino et al., 2005) and modulate inflammatory transcript levels in microglia (Cusimano et al., 2012). The immunomodulatory and trophic properties of grafted NSCs are now well documented (for review see Ottoboni et al., 2015), but the possibility of endogenous SVZdNPs having such functions has never been investigated in the injured brain. Our work provides the first evidence for immunomodulatory functions of endogenous SVZdNPs in the demyelination context. We show that CC areas enriched in SVZdNPs have lower densities of activated microglial cells, and contain subpopulations of microglial cells with an immunomodulatory profile. Nevertheless, we do not rule out the possibility of SVZdNPs acting both locally after mobilization to the lesioned site, and remotely, from their niche.

Microglia are key players in the demyelination/remyelination process, with both deleterious and beneficial properties. In the cuprizone model of demyelination, microglial cells are the first to be activated (Hiremath et al., 1998), and they contribute to OLG death via inflammatory cytokine secretion (Liddelow et al., 2017). However microglia are also required to remove myelin debris,

which would otherwise inhibit remyelination (Napoli and Neumann, 2010; Voß et al., 2012), a prerequisite for the resolution of inflammation and remyelination (Kotter et al., 2006; Lampron et al., 2015). Recent single-cell RNA-sequencing studies have revealed multiple microglial phenotypes, complicating the simplistic dichotomous view of M1 versus M2 phenotypes (Keren-Shaul et al., 2017). Efficient remyelination requires the death of pro-inflammatory microglia and repopulation with pro-regenerative microglia (Lloyd et al., 2019; Miron et al., 2013). In a model of inflammatory demyelinating disease, microglial phagocytic activity is correlated with functional recovery (Yamasaki et al., 2014). We demonstrate here that SVZdNPs are mobilized to the lesion site, where they induce a switch to the immunomodulatory phenotype in microglial cells, thereby promoting the phagocytosis of myelin debris and limiting secondary inflammation-induced demyelination.

We suggest a role for the MFGE8/ITGB3 ligand/receptor pair in the immunomodulatory effects of endogenous SVZdNP. *Mfge8* levels were found to be high in neural progenitors and *Itgb3* was weakly expressed in most microglial cells. Immunolabeling confirmed that the MFGE8 protein was produced and showed its levels to be higher in the lateral than the medial CC. Nevertheless, we cannot strictly impute this to SVZdNPs, because the microglial cells also produced MFGE8. MFGE8 has been shown to recognize phosphatidyl serine "eat me" signal and to bind to the ITGB3 on macrophages mediating the phagocytic clearance of apoptotic cells (Fadok et al., 2000; Hanayama et al., 2002). It has been suggested that MFGE8 acts as a protective factor endowed with immunomodulatory properties (Tan et al., 2015; Xiao et al., 2018), by inhibiting M1 microglia polarization (Shi et al., 2017; Li et al., 2019). We show here that MFGE8 or SVZdNP-conditioned medium enhances the phagocytosis of myelin debris by microglia *in vitro*, this effect of conditioned medium being lost if the SVZdNP are derived from MFGE8$^{-/-}$ mice.

Although this work does not formally demonstrate the role of MFGE8 secreted by SVZdNP *in vivo* in the context of cuprizone-induce demyelination, it provides indirect evidence that endogenous SVZdNP activated by demyelination may help to reduce inflammation and promote the phagocytosis of myelin debris, for instance via MGFE8 secretion. Mobilized SVZdNP could thus provide protection against extensive demyelination and create a local environment more favorable for regeneration.

EXPERIMENTAL PROCEDURES

All experimental and surgical protocols were approved by the ethics committee for animal experimentation (reference 2016071112151400).

Methodological description of immunofluorescence, image analysis and quantification, western blots, and qPCR are provided in supplemental experimental procedures.

Animals

Adult neural progenitors in the SVZ express Nestin, a marker of multipotency. We thus used NestinCre^{ERT2} (Lagace et al., 2007) transgenic mice to trace SVZdNP. Heterozygous Cre mice were crossed with homozygous or heterozygous R26R-YFP (Srinivas et al., 2001) or mTmG (Muzumdar et al., 2007) reporter mice, to generate double-heterozygous offspring for cell lineage analysis. R26R-YFP reporter mice provide cytoplasmic labeling, which is convenient for cell quantification and phenotyping; mTmG reporter mice provide membrane labeling, which is not ideal for cell counting, but very useful for cell morphology analysis, particularly for cells with a complex typical morphology (myelin segments), such as OLG. CX3CR1GFP (Jung et al., 2000) heterozygous transgenic mice were used for the labeling and sorting of microglial cells. CX3CR1 is expressed in both resting and activated microglia. PlpGFP (Le Bras et al., 2005) transgenic mice were used for myelin imaging and quantification in the CC. PLP (proteolipid protein) is a major component of myelin. C57BL/6 (Janvier Laboratories) were used for western blotting.

Tamoxifen injection and demyelination

Tamoxifen (Sigma #T5648; 180 mg/kg) was injected into 6-week-old NestinCre^{ERT2}:R26R-YFP or NestinCre^{ERT2}:mTmG mice every day for 5 consecutive days, to induce recombination and cell labeling. Demyelination was induced by cuprizone (Sigma #C9012) treatment (0.2% in food), for 5 weeks, beginning 2 weeks after the end of the tamoxifen injections. Mice were killed after 3 (W3), 4 (W4), or 5 (W5) weeks of cuprizone treatment or 2 (W5+2) or 4 (W5+4) weeks after the end of cuprizone treatment.

Generation of single-cell suspensions from the CC

For single-cell RNA-sequencing experiments, SVZdNP and microglial cells were isolated from demyelinated CC from NestinCre^{ERT2}:R26R-YFP and CX3CR1GFP mice, respectively. Mice were fed cuprizone for 4 weeks. This time point (between W3 and W5) was chosen as a compromise between the number of cells collected and their differentiation state. Indeed, SVZdNP recruitment remained poor at W3, which would have resulted in the collection of few cells after dissection and FACS. By contrast, SVZdNP were abundant in the CC at W5, but many of these cells already expressed lineage cell markers and could no longer be considered progenitors.

Brains from four to five mice were extracted immediately after perfusion in cold phosphate-buffered saline (PBS) and placed in Hank's balanced salt solution without Ca^{2+} or Mg^{2+} (Invitrogen #14170088). Brains were cut into 500-μm slices with a vibratome (Microm). For SVZdNP single-cell RNA sequencing, the CC was microdissected and cut into three to four pieces to facilitate dissociation. For microglial single-cell RNA sequencing, the medial and lateral CC of each mouse were microdissected separately. The cortex of P1 to P7 WT neonates was used as ballast, to prevent cell loss during successive centrifugation. Cells were dissociated with the Neural Tissue Dissociation Kit (P) (Miltenyi #130-092-628) and automated gentle MACS (37C-NTDK-1 program), in accordance

with the manufacturer's instructions. For the removal of myelin debris, we used Miltenyi magnetic beads (#130-096-733). The cells were resuspended in 500 μL of 0.5% BSA (Sigma #A9418) in PBS.

Single-cell library generation and sequencing

Single-cell library generation (Chromium Single-cell controller; 10X Genomics) and sequencing (NextSeq 500; Illumina) were performed by the HalioDX Company (Luminy, Marseille). The cDNA, library preparation and sequencing all passed quality control tests. NextSeq data were demultiplexed with the 10X Genomics suite Cell Ranger 1.2, and the *mkfastq* function. This first level of analysis generated quality metrics (e.g., Q30, number of reads per sample) and FASTQ files. Cell Ranger 1.2 *count* was then performed on each library (sample) demultiplexed with Cell Ranger 1.2 *mkfastq*. Finally, Cell Ranger 1.2 *count* was performed on a mouse reference genome, determining the number of cells and the number of genes per cell, quantifying gene expression (count tables) and performing t-SNE analysis.

We focused on undifferentiated progenitors, by excluding cells expressing lineage-specific genes: *Plac9b* (ependymal cells), *Aldh1l1* and *S100b* (astrocytes), *Sox10* (OLG) and *Sp9* (neuroblasts), by applying a threshold of 2 (normalized unique molecular identifier (UMI)).

Phagocytosis of myelin debris by microglia

Fluorescently labeled myelin debris was prepared as previously described (Rolfe et al., 2017). Briefly, brains from 10 adult mice were sliced into small pieces, homogenized in 0.32 M sucrose and centrifuged through 0.83 M sucrose (100,000 x *g* 45 min at 4°C). Myelin debris was collected at the interface between the two sucrose concentrations. After two successive Tris buffer rinse/centrifugation steps, the myelin debris pellets were resuspended in PBS (100 mg/mL) and stored at −80°C. The myelin debris was fluorescently labeled by incubation in 50 μM carboxyfluorescein succinimidyl ester (CFSE; Invitrogen #C34570) for 30 min at room temperature, washed (100 mM glycine in PBS) three times, and centrifuged (14,800 × *g*, 10 min 4°C); the fluorescent myelin debris was finally suspended in sterile PBS (100 mg/mL).

We developed a BV2 cell line (mouse brain microglial cells) stably expressing dsRed ("BV2-DsRed") to facilitate the visualization of myelin debris phagocytosis. BV2 or BV2-DsRed cells were used to seed 4-well Lab-Tek (Sigma #C6932) plates at a density of 200,000 cells/mL. After 24 h, we added 5 μL rmMFGE8 (500 ng/mL; R&D #2805-MF-050) to the culture medium (or PBS for control). Then, 1 h after MFGE8 addition, CFSE-labeled myelin debris (1 mg/mL) was added to the culture, which was incubated for a further 3 hours. The cells were fixed by incubation in 4% paraformaldehyde for 30 min, rinsed, and their nuclei were labeled by incubation for 5 min in Hoechst stain. We took 10 photographs per well at ×20 magnification, and the proportion of microglia engaged in phagocytosis was quantified.

The same experiment was also performed with neurosphere-conditioned medium in place of MFGE8 treatment.

Statistical analyses

Nonparametric Mann-Whitney and Wilcoxon tests were used for two-group comparisons (unpaired and paired samples, respectively). For the comparison of multiple groups, ANOVA by score permutation was performed, followed by Kruskal-Wallis tests with StatXact software (Cytel Studio). Differences were considered significant if $p < 0.05$ (*), and highly significant if $p < 0.01$ (**).

Data and code availability

The processed data of single-cell RNA sequencing are deposited in the NCBI Gene Expression Omnibus (GEO: GSE144201 and GEO: GSE144202, for SVZdNP and microglia, respectively).

SUPPLEMENTAL INFORMATION

Supplemental information can be found online at https://doi.org/10.1016/j.stemcr.2021.05.002.

AUTHOR CONTRIBUTIONS

B.B. performed most of the experiments and analyzed the data, with the help of K.M. and O.M.; F.D. performed bioinformatics analyses on single-cell RNA sequencing data; P.D. and M.C. directed the study and wrote the manuscript.

ACKNOWLEDGMENTS

We thank C. Maurange, C. Faivre Sarrailh, and L. Kerkerian Le Goff for critical reading of the manuscript. This work was funded by CNRS, Aix-Marseille University, the *Fondation pour la Recherche Médicale* (DEC 20140329501) and the ARSEP foundation. We also thank France-bioimaging/PICSL infrastructure (ANR-10-INSB-04-01). This work received support from the French government under the "Investissements d'Avenir" program, Initiative d'Excellence d'Aix-Marseille Université via AMidex funding NeuroMarseille AMX-19-IET-004, and NeuroSchool ANR-17-EURE-0029. BB was funded by the ANR and an ARSEP fellowship.

Received: February 8, 2021
Revised: May 5, 2021
Accepted: May 6, 2021
Published: June 3, 2021

REFERENCES

Aguirre, A., Dupree, J.L., Mangin, J.M., and Gallo, V. (2007). A functional role for EGFR signaling in myelination and remyelination. Nat. Neurosci. *10*, 990–1002.

Albert, M., Antel, J., Brück, W., and Stadelmann, C. (2007). Extensive cortical remyelination in patients with chronic multiple sclerosis. Brain Pathol. *17*, 129–138.

Boockvar, J.A., Schouten, J., Royo, N., Millard, M., Spangler, Z., Castelbuono, D., Snyder, E., O'Rourke, D., and McIntosh, T. (2005). Experimental traumatic brain injury modulates the survival, migration, and terminal phenotype of transplanted epidermal growth factor receptor-activated neural stem cells. Neurosurgery *56*, 163–171.

Brousse, B., Magalon, K., Durbec, P., and Cayre, M. (2015). Region and dynamic specificities of adult neural stem cells and

oligodendrocyte precursors in myelin regeneration in the mouse brain. Biol. Open *4*, 980–992.

Butti, E., Bacigaluppi, M., Chaabane, L., Ruffini, F., Brambilla, E., Berera, G., Montonati, C., Quattrini, A., and Martino, G. (2019). Neural stem cells of the subventricular zone contribute to neuroprotection of the corpus callosum after cuprizone-induced demyelination. J. Neurosci. *39*, 5481–5492.

Carbajal, K.S., Schaumburg, C., Strieter, R., Kane, J., and Lane, T.E. (2010). Migration of engrafted neural stem cells is mediated by CXCL12 signaling through CXCR4 in a viral model of multiple sclerosis. Proc. Natl. Acad. Sci. U S A *107*, 11068–11073.

Chrzanowski, U., Schmitz, C., Horn-Bochtler, A., Nack, A., and Kipp, M. (2019). Evaluation strategy to determine reliable demyelination in the cuprizone model. Metab. Brain Dis. *34*, 681–685.

Chu, F., Shi, M., Zheng, C., Shen, D., Zhu, J., Zhenga, X., and Cui, L. (2018). The roles of macrophages and microglia in multiple sclerosis and experimental autoimmune encephalomyelitis. J. Neuroimmunol. *318*, 1–7.

Cusimano, M., Biziato, D., Brambilla, E., Donegà, M., Alfaro-Cervello, C., Snider, S., Salani, G., Pucci, F., Comi, G., Garcia-Verdugo, J.M., et al. (2012). Transplanted neural stem/precursor cells instruct phagocytes and reduce secondary tissue damage in the injured spinal cord. Brain A J. Neurol. *135*, 447–460.

De Feo, D., Merlini, A., Laterza, C., and Martino, G. (2012). Neural stem cell transplantation in central nervous system disorders: from cell replacement to neuroprotection. Curr. Opin. Neurol. *25*, 322–333.

De Gioia, R., Biella, F., Citterio, G., Rizzo, F., Abati, E., Nizzardo, M., Bresolin, N., Comi, G.P., and Corti, S. (2020). Neural stem cell transplantation for neurodegenerative diseases. Int. J. Mol. Sci. *21*, 3103.

Deroide, N., Li, X., Lerouet, D., Van Vre, E., Baker, L., Harrison, J., Poittevin, M., Masters, L., Nih, L., Margaill, I., et al. (2013). MFGE8 inhibits inflammasome-induced IL-1beta production and limits postischemic cerebral injury. J. Clin. Invest. *123*, 1176–1181.

Doetsch, F., Caillé, I., Lim, D.A., García-Verdugo, J.M., and Alvarez-Buylla, A. (1999). Subventricular zone astrocytes are neural stem cells in the adult mammalian brain. Cell *97*, 703–716.

El Waly, B., Cayre, M., and Durbec, P. (2018). Promoting myelin repair through *in vivo* neuroblast reprogramming. Stem Cell Reports *10*, 1492–1504.

Fadok, V.A., Bratton, D.L., Rose, D.M., Pearson, A., Ezekewitz, R.A., and Henson, P.M. (2000). A receptor for phosphatidylserine-specific clearance of apoptotic cells. Nature *405*, 85–90.

Franklin, R.J., Gilson, J.M., and Blakemore, W.F. (1997). Local recruitment of remyelinating cells in the repair of demyelination in the central nervous system. J. Neurosci. Res. *50*, 337–344.

Gao, J., Grill, R.J., Dunn, T.J., Bedi, S., Labastida, J.A., Hetz, R.A., Xue, H., Thonhoff, J.R., DeWitt, D.S., Prough, D.S., et al. (2016). Human neural stem cell transplantation-mediated alteration of microglial/macrophage phenotypes after traumatic brain injury. Cell Transplant. *25*, 1863–1877.

Gensert, J.M., and Goldman, J.E. (1997). Endogenous progenitors remyelinate demyelinated axons in the adult CNS. Neuron *19*, 197–203.

Goldberg, N.R.S., Caesar, J., Park, A., Sedgh, S., Finogenov, G., Masliah, E., Davis, J., and Blurton-Jones, M. (2015). Neural stem cells rescue cognitive and motor dysfunction in a transgenic model of dementia with Lewy bodies through a BDNF-dependent mechanism. Stem Cell Reports *5*, 791–804.

Hanayama, R., Tanaka, M., Miwa, K., Shinohara, A., Iwamatsu, A., and Nagata, S. (2002). Identification of a factor that links apoptotic cells to phagocytes. Nature *417*, 182–187.

Hiremath, M.M., Saito, Y., Knapp, G.W., Ting, J.P., Suzuki, K., and Matsushima, G.K. (1998). Microglial/macrophage accumulation during cuprizone-induced demyelination in C57BL/6 mice. J. Neuroimmunol. *92*, 38–49.

Jablonska, B., Aguirre, A., Raymond, M., Szabo, G., Kitabatake, Y., Sailor, K.A., Ming, G.-L., Song, H., and Gallo, V. (2010). Chordin-induced lineage plasticity of adult SVZ neuroblasts after demyelination. Nat. Neurosci. *13*, 541–550.

Jung, S., Aliberti, J., Graemmel, P., Sunshine, M.J., Kreutzberg, G.W., Sher, A., and Littman, D.R. (2000). Analysis of fractalkine receptor CX(3)CR1 function by targeted deletion and green fluorescent protein reporter gene insertion. Mol. Cell Biol. *20*, 4106–4114.

Kazanis, I., Evans, K.A., Andreopoulou, E., Dimitriou, C., Koutsakis, C., Karadottir, R.T., and Franklin, R.J.M. (2017). Subependymal zone-derived oligodendroblasts respond to focal demyelination but fail to generate myelin in young and aged mice. Stem Cell Reports *8*, 685–700.

Keren-Shaul, H., Spinrad, A., Weiner, A., Matcovitch-Natan, O., Dvir-Szternfeld, R., Ulland, T.K., David, E., Baruch, K., Lara-Astaiso, D., Toth, B., et al. (2017). A unique microglia type associated with restricting development of Alzheimer's disease. Cell *169*, 1276–1290.e17.

Kokaia, Z., Martino, G., Schwartz, M., and Lindvall, O. (2012). Cross-talk between neural stem cells and immune cells: the key to better brain repair? Nat. Neurosci. *15*, 1078–1087.

Kotter, M.R., Li, W.-W., Zhao, C., and Franklin, R.J.M. (2006). Myelin impairs CNS remyelination by inhibiting oligodendrocyte precursor cell differentiation. J. Neurosci. *26*, 328–332.

Lagace, D.C., Whitman, M.C., Noonan, M.A., Ables, J.L., DeCarolis, N.A., Arguello, A.A., Donovan, M.H., Fischer, S.J., Farnbauch, L.A., Beech, R.D., et al. (2007). Dynamic contribution of nestin-expressing stem cells to adult neurogenesis. J. Neurosci. *27*, 12623–12629.

Lampron, A., Larochelle, A., Laflamme, N., Préfontaine, P., Plante, M.-M., Sánchez, M.G., Yong, V.W., Stys, P.K., Tremblay, M.-È., and Rivest, S. (2015). Inefficient clearance of myelin debris by microglia impairs remyelinating processes. J. Exp. Med. *212*, 481–495.

Le Bras, B., Chatzopoulou, E., Heydon, K., Martinez, S., Ikenaka, K., Prestoz, L., Spassky, N., Zalc, B., and Thomas, J.L. (2005). Oligodendrocyte development in the embryonic brain: the contribution of the plp lineage. Int. J. Dev. Biol. *49*, 209–220.

Li, J., Xu, X., Cai, X., Weng, Y., Wang, Y., Shen, Q., and Shi, X. (2019). Milk fat globule-epidermal growth factor-factor 8 reverses lipopolysaccharide-induced microglial oxidative stress. In Oxidative Medicine and Cellular Longevity (Hindawi), pp. 1–8.

Liddelow, S.A., Guttenplan, K.A., Clarke, L.E., Bennett, F.C., Bohlen, C.J., Schirmer, L., Bennett, M.L., Münch, A.E., Chung, W.-S.,

Peterson, T.C., et al. (2017). Neurotoxic reactive astrocytes are induced by activated microglia. Nature *541*, 481–487.

Liu, F., Chen, Y., Hu, Q., Li, B., Tang, J., He, Y., Guo, Z., Feng, H., Tang, J., and Zhang, J.H. (2015). MFGE8/Integrin beta3 pathway alleviates apoptosis and inflammation in early brain injury after subarachnoid hemorrhage in rats. Exp. Neurol. *272*, 120–127.

Liu, J., Hjorth, E., Zhu, M., Calzarossa, C., Samuelsson, E.B., Schultzberg, M., and Akesson, E. (2013). Interplay between human microglia and neural stem/progenitor cells in an allogeneic co-culture model. J. Cell Mol. Med. *17*, 1434–1443.

Lloyd, A.F., Davies, C.L., Holloway, R.K., Labrak, Y., Ireland, G., Carradori, D., Dillenburg, A., Borger, E., Soong, D., Richardson, J.C., et al. (2019). Central nervous system regeneration is driven by microglia necroptosis and repopulation. Nat. Neurosci. *22*, 1046–1052.

Marteyn, A., Sarrazin, N., Yan, J., Bachelin, C., Deboux, C., Santin, M.D., Gressens, P., Zujovic, V., and Baron-Van Evercooren, A. (2016). Modulation of the innate immune response by human neural precursors prevails over oligodendrocyte progenitor remyelination to rescue a severe model of Pelizaeus-Merzbacher disease. Stem Cells *34*, 984–996.

Martino, G., Pluchino, S., Bonfanti, L., and Schwartz, M. (2011). Brain regeneration in physiology and pathology: the immune signature driving therapeutic plasticity of neural stem cells. Physiol. Rev. *91*, 1281–1304.

Menn, B., Garcia-Verdugo, J.M., Yaschine, C., Gonzalez-Perez, O., Rowitch, D., and Alvarez-Buylla, A. (2006). Origin of oligodendrocytes in the subventricular zone of the adult brain. J. Neurosci. *26*, 7907–7918.

Miron, V.E., Boyd, A., Zhao, J.-W., Yuen, T.J., Ruckh, J.M., Shadrach, J.L., van Wijngaarden, P., Wagers, A.J., Williams, A., Franklin, R.J.M., and Ffrench-Constant, C. (2013). M2 microglia and macrophages drive oligodendrocyte differentiation during CNS remyelination. Nat. Neurosci. *16*, 1211–1218.

Muzumdar, M.D., Tasic, B., Miyamichi, K., Li, L., and Luo, L. (2007). A global double-fluorescent Cre reporter mouse. Genesis *45*, 593–605.

Nait-Oumesmar, B., Decker, L., Lachapelle, F., Avellana-Adalid, V., Bachelin, C., and Baron-Van Evercooren, A. (1999). Progenitor cells of the adult mouse subventricular zone proliferate, migrate and differentiate into oligodendrocytes after demyelination. Eur. J. Neurosci. *11*, 4357–4366.

Napoli, I., and Neumann, H. (2010). Protective effects of microglia in multiple sclerosis. Exp. Neurol. *225*, 24–28.

Ottoboni, L., De Feo, D., Merlini, A., and Martino, G. (2015). Commonalities in immune modulation between mesenchymal stem cells (MSCs) and neural/precursor cells (NPCs). Immunol. Lett. *68*, 228–239.

Patrikios, P., Stadelmann, C., Kutzelnigg, A., Rauschka, H., Schmidbauer, M., Laursen, H., Sorensen, P.S., Brück, W., Lucchinetti, C., and Lassmann, H. (2006). Remyelination is extensive in a subset of multiple sclerosis patients. Brain A J. Neurol. *129*, 3165–3172.

Peferoen, L.A.N., Vogel, D.Y.S., Ummenthum, K., Breur, M., Heijnen, P.D.A.M., Gerritsen, W.H., Peferoen-Baert, R.M.B., van der Valk, P., Dijkstra, C.D., and Amor, S. (2015). Activation status of human microglia is dependent on lesion formation stage and remyelination in multiple sclerosis. J. Neuropathol. Exp. Neurol. *74*, 48–63.

Picard-Riera, N., Decker, L., Delarasse, C., Goude, K., Nait-Oumesmar, B., Liblau, R., Pham-Dinh, D., and Baron-Van Evercooren, A. (2002). Experimental autoimmune encephalomyelitis mobilizes neural progenitors from the subventricular zone to undergo oligodendrogenesis in adult mice. Proc. Natl. Acad. Sci. U S A *99*, 13211–13216.

Pluchino, S., Gritti, A., Blezer, E., Amadio, S., Brambilla, E., Borsellino, G., Cossetti, C., Del Carro, U., Comi, G., t Hart, B., et al. (2009). Human neural stem cells ameliorate autoimmune encephalomyelitis in non-human primates. Ann. Neurol. *66*, 343–354.

Pluchino, S., Zanotti, L., Rossi, B., Brambilla, E., Ottoboni, L., Salani, G., Martinello, M., Cattalini, A., Bergami, A., Furlan, R., et al. (2005). Neurosphere-derived multipotent precursors promote neuroprotection by an immunomodulatory mechanism. Nature *436*, 266–271.

Poliani, P.L., Wang, Y., Fontana, E., Robinette, M.L., Yamanishi, Y., Gilfillan, S., and Colonna, M. (2015). TREM2 sustains microglial expansion during aging and response to demyelination. J. Clin. Invest. *125*, 2161–2170.

Rolfe, A.J., Bosco, D.B., Broussard, E.N., and Ren, Y. (2017). *In vitro* phagocytosis of myelin debris by bone marrow-derived macrophages. J. Vis. Exp. *130*, 56332.

Serwanski, D.R., Rasmussen, A.L., Brunquell, C.B., Perkins, S.S., and Nishiyama, A. (2018). Sequential contribution of parenchymal and neural stem cell-derived oligodendrocyte precursor cells toward remyelination. Neuroglia *1*, 91–105.

Shi, X., Cai, X., Di, W., Li, J., Xu, X., Zhang, A., Qi, W., Zhou, Z., and Fang, Y. (2017). MFG-E8 selectively inhibited Aβ-induced microglial M1 polarization via NF-κB and PI3K-Akt pathways. Mol Neurobiol *54*, 7777–7788. https://doi.org/10.1007/s12035-016-0255-y.

Srinivas, S., Watanabe, T., Lin, C.S., William, C.M., Tanabe, Y., Jessell, T.M., and Costantini, F. (2001). Cre reporter strains produced by targeted insertion of EYFP and ECFP into the ROSA26 locus. BMC Dev. Biol. *1*, 4.

Steelman, A.J., Thompson, J.P., and Li, J. (2012). Demyelination and remyelination in anatomically distinct regions of the corpus callosum following cuprizone intoxication. Neurosci. Res. *72*, 32–42.

Tan, Y., AlKhamees, B., Jia, D., Li, L., Couture, J.F., Figeys, D., Jinushi, M., and Wang, L. (2015). MFG-E8 is critical for embryonic stem cell-mediated T cell immunomodulation. Stem Cell Reports *5*, 741–752.

Vogel, D.Y., Vereyken, E.J., Glim, J.E., Heijnen, P.D., Moeton, M., van der Valk, P., Amor, S., Teunissen, C.E., van Horssen, J., and Dijkstra, C.D. (2013). Macrophages in inflammatory multiple sclerosis lesions have an intermediate activation status. J. Neuroinflamm. *10*, 35.

Voß, E.V., Škuljec, J., Gudi, V., Skripuletz, T., Pul, R., Trebst, C., and Stangel, M. (2012). Characterisation of microglia during de- and remyelination: can they create a repair promoting environment? Neurobiol. Dis. *45*, 519–528.

Wu, H.M., Zhang, L.F., Ding, P.S., Liu, Y.J., Wu, X., and Zhou, J.N. (2014). Microglial activation mediates host neuronal survival induced by neural stem cells. J. Cell Mol. Med. *18*, 1300–1312.

Xiao, Y., Li, G., Chen, Y., Zuo, Y., Rashid, K., He, T., Feng, H., Zhang, J.H., and Liu, F. (2018). Milk fat globule-epidermal growth factor-8 pretreatment attenuates apoptosis and inflammation via the integrin-beta3 pathway after surgical brain injury in rats. Front. Neurol. *9*, 96.

Xing, Y.L., Röth, P.T., Stratton, J.A.S., Chuang, B.H.A., Danne, J., Ellis, S.L., Ng, S.W., Kilpatrick, T.J., and Merson, T.D. (2014). Adult neural precursor cells from the subventricular zone contribute significantly to oligodendrocyte regeneration and remyelination. J. Neurosci. *34*, 14128–14146.

Yamasaki, R., Lu, H., Butovsky, O., Ohno, N., Rietsch, A.M., Cialic, R., Wu, P.M., Doykan, C.E., Lin, J., Cotleur, A.C., et al. (2014). Differential roles of microglia and monocytes in the inflamed central nervous system. J. Exp. Med. *211*, 1533–1549.

Zawadzka, M., Rivers, L.E., Fancy, S.P.J., Zhao, C., Tripathi, R., Jamen, F., Young, K., Goncharevich, A., Pohl, H., Rizzi, M., et al. (2010). CNS-resident glial progenitor/stem cells produce Schwann cells as well as oligodendrocytes during repair of CNS demyelination. Cell Stem Cell *6*, 578–590.

Zhang, Q., Wu, H.H., Wang, Y., Gu, G.J., Zhang, W., and Xia, R. (2016). Neural stem cell transplantation decreases neuroinflammation in a transgenic mouse model of Alzheimer's disease. J. Neurochem. *136*, 815–825.

Zhang, Y., Cai, L., Fan, K., Fan, B., Li, N., Gao, W., Yang, X., and Ma, J. (2019). The spatial and temporal characters of demyelination and remyelination in the cuprizone animal model. Anat. Rec. (Hoboken) *302*, 2020–2029.

Zuo, F.X., Bao, X.J., Sun, X.C., Wu, J., Bai, Q.R., Chen, G., Li, X.Y., Zhou, Q.Y., Yang, Y.F., Shen, Q., and Wang, R.Z. (2015). Transplantation of human neural stem cells in a Parkinsonian model exerts neuroprotection via regulation of the host microenvironment. Int. J. Mol. Sci. *16*, 26473–26492.